Control of recollection by slow gamma dominating medium gamma in hippocampus CA1

Authors:

Dino Dvorak[1], Basma Radwan[1], Fraser T. Sparks[1], Zoe Nicole Talbot[2], André A. Fenton[1,3,4]

Affiliations

[1]Center for Neural Science, New York University, New York, 10003, USA

[2]School of Medicine, New York University, New York, NY 10016, USA

[3]Neuroscience Institute at the New York University Langone Medical Center, New York, NY 10016, USA

[4]Department of Physiology and Pharmacology, The Robert F. Furchgott Center for Neural & Behavioral Science, State University of New York, Downstate Medical Center, Brooklyn, New York, 11203, USA.

Author for Correspondence:

Prof. André Fenton
Neurobiology of Cognition Laboratory
Center for Neural Science, Room 980
New York University
4 Washington Place
New York, NY 10003-662
afenton@nyu.edu

ABSTRACT

Behavior is used to assess memory and cognitive deficits in animals like Fmr1-null mice that model Fragile-X Syndrome, but behavior is a proxy for unknown neural events that define cognitive variables like recollection. We identified an electrophysiological signature of recollection in mouse dorsal CA1 hippocampus. During a shocked-place avoidance task, slow-gamma (SG: 30-60 Hz) dominates medium-gamma (MG: 60-90 Hz) oscillations 2-3 seconds before successful avoidance, but not failures. Wild-type but not Fmr1-null mice adapt to relocating the shock; concurrently, SG/MG maxima ($SG_{dominance}$) decrease in wild-type but not in cognitively inflexible Fmr1-null mice. During $SG_{dominance}$ events, place cell ensembles represent distant locations; during place avoidance, these are avoided places. During shock relocation, wild-type ensembles represent distant locations near the currently-correct shock zone but Fmr1-null ensembles represent the formerly-correct zone. These findings indicate that recollection occurs when CA1 slow gamma dominates medium gamma, and that accurate recollection of inappropriate memories explains Fmr1-null cognitive inflexibility.

INTRODUCTION

The hippocampus is crucial for both learning and remembering information, especially about space [1], and because the same place-representing neurons participate in both processes [2-7], it is unknown what neural events control whether hippocampal neurons are encoding current experience or recollecting information from memory [8]. A prominent “communication-through-coherence” [9-12] or “routing-by-synchrony” hypothesis asserts that activity in CA1 switches between an information acquiring mode associated with medium 60-90 Hz gamma oscillations that synchronize hippocampus output with neocortical input and a separate long-term memory recollection mode associated with slow 30-60 Hz gamma oscillations that synchronize CA1 output with intrahippocampal CA3→CA1 inputs [12, 13]. Gamma oscillations are generated by local interneurons [14-17] and the local CA1 GABAergic

currents that underlie gamma oscillations are effectively driven by tonic excitation, as described by pyramidal interneuron network gamma (PING) models of gamma generation [18-20]. Furthermore, tonic inputs to PING as well as interneuron network gamma (ING) models can locally generate distinct lower and higher frequency gammas by local competition between distinct interneuron populations with correspondingly long and short lasting post-synaptic inhibition [21]. Because CA1 receives two anatomically distinct inputs [22, 23] and each mediates both dendritic excitation and feedforward inhibition [24], routing-by-synchrony hypotheses predict that during long-term memory recall the CA3-associated slow gamma input will outcompete the entorhinal cortex-associated medium gamma input for control of CA1 output.

We test this prediction and find in freely-behaving mice solving a place task, that slow and medium gamma oscillations are concurrent in mouse CA1, but a transient dominance of slow gamma oscillations over medium gamma oscillations signals recollection. This slow gamma dominance lasts several hundred milliseconds and occurs on average every ~9 seconds, both when mice are active or still. Increased and decreased rates of slow gamma dominance predicts accurate, failed and changed place memory in wild-type mice, as well as cognitive inflexibility in a Fmr1-null mutant mouse model of Fragile-X Syndrome intellectual disability, associated with high prevalence of autism. During slow gamma dominance, place cell ensemble discharge represents distant locations, and during place avoidance tasks these distant locations are the vicinity of the shock zone that the mouse learned to avoid. However, when Fmr1-null mice express cognitive inflexibility by continuing to avoid the formerly correct and now incorrect place, these slow gamma dominance events are excessive and predictive of place cell representations of formerly-correct shock-zone location memories. Because gamma oscillations are generated by local inhibitory synapses, and consistent with theory [21], these results point to local biases in competing gamma-generating inhibitory events as the potential origin of distinct information and long-term memory processing modes, such as recollection.

RESULTS

Identifying recollection events prior to active avoidance

We began by identifying when mice were likely to recall the location of shock during training in variants of the active place avoidance task [Fig. 1A; 25]. Periods of stillness, when the mouse is passively carried towards the shock zone, are interrupted by active avoidances (Fig. 1B), indicating successful recollection of the shock location and identifying times with a high likelihood of recollection (Fig. 1).

The routing-by-synchrony hypothesis [12, 13] predicts that CA3-driven slow gamma (30-60 Hz) oscillations will transiently dominate neocortex-driven medium gamma (60-90 Hz) oscillations when the mouse is recollecting the shock zone location (Fig. 1C). Concurrent local field potentials (LFPs), reflecting synchronous synaptic activity within the dorsal hippocampus, were recorded at the perisomatic region of CA1 and examined during these behavioral segments. The LFP state was mostly in theta, although somewhat lower amplitude during stillness (supplementary information Fig. S1A), as is typical for spatially alert stillness [26]. At *stratum pyramidale*, slow and medium gamma power could be separated by their different phase relationships to theta but less so by their frequency content during both stillness and active locomotion (Fig. S2C,D). Importantly, the rate of sharp-wave associated ripples during these pre-avoidance periods of stillness was no different than the overall stillness ripple rate (supplementary information Fig. S1B).

It was reported that theta oscillations in the *stratum pyramidale* LFP of the freely-behaving rat are predominantly concurrent with either 25-50 Hz CA3-associated gamma or 65-140 Hz entorhinal cortex layer 3 (ECIII) gamma oscillations, but rarely both. However, when both gammas occur in the same theta oscillation, slower gamma is at an earlier theta phase than the faster gamma [12]. In contrast to recordings in the rat, we find that in the mouse, both slow and medium gamma oscillations frequently occur within single theta oscillations in the *stratum pyramidale* LFP (see supplementary

information Fig. S2E and Fig. S3D). It is only after selecting oscillations with the largest power that theta cycles can be shown to be dominated by either slow or medium gamma oscillations, but this is likely an artifact of rejecting most oscillations since only a single supra-threshold gamma oscillation occurs within a single theta cycle when the threshold is > 2 S.D. (supplementary information Fig. S3D). Furthermore, we also find in the mouse that slow gamma oscillations occur close to the theta trough, while medium gamma oscillations occur close to the theta peak (supplementary information Fig. S2C,D). This is opposite to the relationship reported by Colgin et al., 2009, but is similar to what is reported by other work in rats [14] and mouse [16, 27]. While input-specific oscillatory components in CA1 can be de-mixed using high-density silicon probe recordings with current source density (CSD) analysis [27] (see also Supplementary information Fig. S2A-C) or independent component analysis [28], here we exploit that both slow and medium gamma oscillations can be identified in CA1 *stratum pyramidale*, which is both the target of place cell recordings, and the basis of virtually all the data upon which the routing-by-synchrony hypotheses are based.

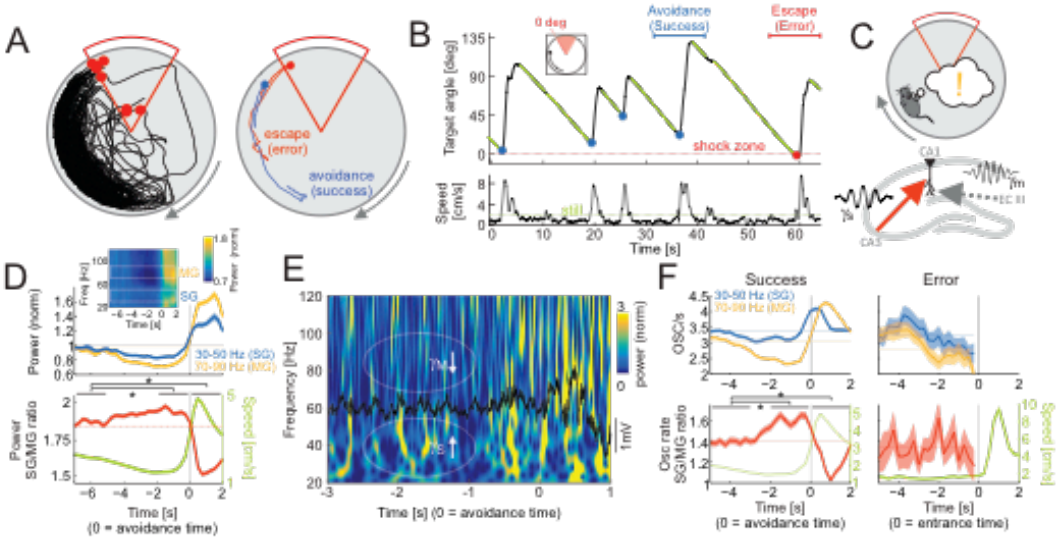

Figure 1. Slow gamma dominates medium gamma prior to successful place avoidance. A left) Typical 30-min path during the third active place avoidance training session. Shocks are shown as red dots. A

right) Example of avoidance (success; blue line) and escape after receiving a shock (error; red line). B top) Time profile of the angular distance to the leading edge of the shock zone showing a typical saw-tooth avoidance pattern during ~60 s. Periods of stillness (green), when the mouse is passively carried towards the shock zone are interrupted by active avoidances (blue dots). Entrance to the shock zone is marked as a red dot. The horizontal blue and red lines mark time intervals of the example avoidance and escape from panel A right. Red dotted line marks the leading edge of the shock zone. B bottom) Speed profile during the same ~60-s interval showing that speed increases during avoidances and escapes. The stillness threshold is shown as a green dotted line at 2 cm/s. C) Schematic depiction of the working hypothesis – as the mouse approaches the shock zone (top), slow gamma driven by CA3 inputs transiently dominates medium gamma driven by ECIII inputs causing recollection of shock zone location. D top) Average power of slow gamma (blue; 30-50 Hz) and medium gamma (yellow; 70-90 Hz) in the LFP around the time of avoidance initiation (T=0). Mean powers are displayed as dotted lines. Inset shows average of normalized power across 20-120 Hz around avoidance initiation. Representative slow and medium gamma bands are marked by white rectangles. D bottom) The average ratio of slow to medium gamma power (red line) around avoidance initiation. The mean power ratio is shown as a dotted line. The corresponding average speed profile is shown in green. Data are represented as average ± SEM. *p < 0.05 relative to baseline (-7..-5 s). E) The time-frequency representation of a 4-s exemple LFP (overlayed in black) around the initiation of an avoidance start (T=0 marks avoidance initiation). Notice the relative reduction in number of medium gamma (60-90 Hz) oscillatory events relative to slow gamma (30-60 Hz) events prior to the avoidance (T ~ -2 s) compared to times during the active avoidance (T > 0 s). F left, top) Average event rates for slow gamma (blue; 30-50 Hz) and medium gamma (yellow; 70-90 Hz) oscillations around the time of avoidance initiation (T=0). Mean rates are displayed as dotted lines. F left, bottom) The average ratio of slow to medium gamma event rates (red line) around avoidance initiation. The mean ratio is shown as a dotted line. The corresponding average

speed profile is shown in green. F right) Same as F left but for Avoidance errors. Data are represented as average ± SEM. *p < 0.05 relative to baseline (-5..-3 s).

We began by comparing power in representative frequency bands for slow gamma (30-50 Hz) and medium gamma (70-90 Hz) and their respective power ratio (Fig. 1D). Before the mouse initiated avoidance movements, the ratio of slow to medium gamma power progressively increased from ~5s prior to the initiation of avoidance movements with maximum ratio occurring ~1 s prior to the active avoidance. This relationship was confirmed with one-way ANOVA ($F_{2,5168}$ = 294.84; p < 0.0001) of the differences between three time intervals (-7..-5 s, -2..0 s and 0..2 s) around the avoidance onset. Post-hoc Dunnett's tests confirmed significant differences from the -7..-5 s baseline interval for intervals just before (-2..0 s) and just after (0..2 s) the initiation of active avoidance (p < 0.001 in both cases). The power ratio was strongly negatively correlated with speed (Fig. 1D bottom; Pearson's correlation r = -0.25, p < 0.0001) as has been reported [29]. Because changes in speed confound associating these changes in the LFP with recollection, we examined alternative approaches for characterizing gamma changes in the LFP that are minimally impacted by speed and instead emphasize the internal cognitive information processing upon which the routing-by-synchrony hypothesis is based.

The routing-by-synchrony hypothesis also predicts that information between two networks is relayed most effectively during high-power, synchronized oscillatory states in contrast to all non-oscillatory activity which gives rise to the 1/f power spectra of LFP or EEG signals [30, see also Supplementary material Fig. S1B]. Because the present work relies on comparing oscillations of different frequency bands, to avoid potentially misleading estimates of the relative strength of oscillations from 1/f organized power spectra, we took advantage of our prior work and discretized continuous LFP signals into frequency-specific oscillatory events and their rates [31]. Oscillatory events were detected as local power maxima in the z-score normalized, wavelet-transformed LFP signal (Fig. S2E; also refer to

Supplemental material Fig. S3 for discussion about threshold setting for event detection). To compute rates of oscillatory events, we first selected representative frequency bands for slow gamma (30-50 Hz) and medium gamma events (70-90 Hz; refer to Supplemental material Fig. S3 for discussion about band selection) and then computed event rates as the number of detected events in a given frequency range above 2.5 S.D. power at *stratum pyramidale* in 1000-ms long windows advanced by 250ms consistent with prior routing-by-synchrony studies [7, 12, 32].

The ratio of slow to medium gamma oscillation events is maximal when recollection likelihood is high

The session-specific slow gamma (SG) and medium gamma (MG) oscillation rates and the SG/MG ratios were examined around the time of avoidances of the initial location of shock. The medium gamma oscillation rate decreased with the minimum occurring 2 – 0.5 s before avoidance onset (Fig. 1E, Fig. 1F left). Slow gamma had a less pronounced decrease and could even increase before avoidance onset. Slow gamma increased after avoidance onset, peaking about 500 ms afterwards, preceding medium gamma, which peaked at 750 ms. In contrast to the power ratio (Fig. 1D), the SG/MG ratio was only weakly correlated with speed ($r = - 0.09$, $p < 0.0001$). The SG/MG ratio was maximal 1-2 seconds before and it was minimal ~1 s after avoidance onset (Fig. 1F). These relationships were confirmed with one-way ANOVA ($F_{2,4134} = 54.22$; $p < 0.0001$) on the SG/MG ratios between three time intervals (-5..-3 s, -2..0 s and 0..2 s) around avoidance onset. Post-hoc Dunnett's test confirmed significant differences from the -5..-3 s baseline interval, for intervals just before (-2..0 s) and just after (0..2 s) the initiation of active avoidance ($p < 0.001$ in both cases). The comparison was not significant ($F_{2,120} = 0.36$; $p = 0.69$) when the mouse failed to actively avoid shock but nonetheless initiated running away from the shock zone upon being shocked (Fig. 1F right). Because this slow gamma dominance over medium gamma (SG_{dom}) was identified during a few seconds of stillness prior to avoidance of the shock location, it is possible that

SG_{dom} either indicates momentary recollection of the shock locations, or preparation (initiation) of locomotion.

Slow gamma dominance predicts successful place avoidance

We then investigated whether the rates of slow or medium gamma oscillations, or their ratio indexed behavior associated with recollection or initiation of movement *per se*. We first examined the time series of the SG/MG ratio without restricting analysis to peri-avoidance episodes with preceding stillness (Fig. 2). To compute time intervals between the SG/MG maxima that define SG_{dom}, we first detected local peaks in the SG/MG ratio series with amplitude > 1 (i.e. SG > MG) and then selected the subset of maxima with prominence (amplitude difference between maxima to the preceding and following minima) > 1. This step excluded short intervals resulting in multiple peaks in a sequence (see Fig. 2A).

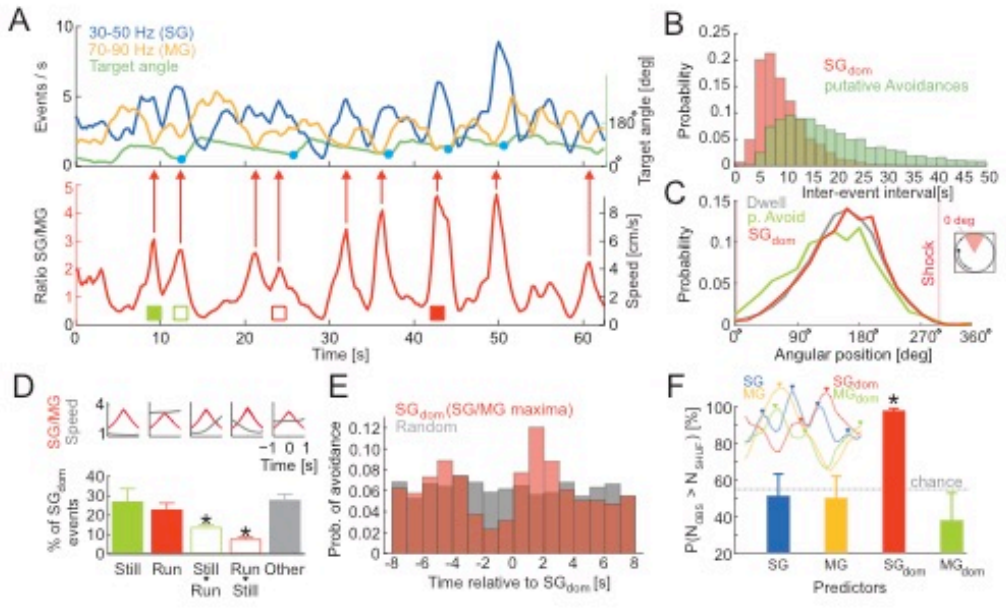

Figure 2. Slow to medium gamma maxima predict active avoidance. A top) Time series of slow gamma and medium gamma event rates and the angular distance of a mouse from the leading edge of the shock zone. Avoidances are marked by blue dots. The leading edge of the shock zone corresponds to 0°.

A bottom) Time series of slow to medium gamma ratio (SG/MG) with local maxima (SG_{dom}) indicated (red arrows). B) Probability distributiosn of inter-event intervals for consecutive SG_{dom} events and putative avoidances during training sessions. C) Angular distributions of a mouse's location, locations of avoidances, and locations of SG_{dom} events. D) Proportions of SG_{dom} events detected during different behavioral states – (from left) stillness, running, acceleration, deceleration and other. Average SG/MG ratio and speed in 2-s windows around SG/FG maxima is shown at the top. Corresponding examples of behavioral states is marked by colored squares in A bottom. *$p < 0.05$ relative to stillness. E) Probability of observing an avoidance relative to a SG_{dom} event and randomly selected times. F) The probability of predicting avoidances by chance (after randomly shifting the time stamps of detected maxima), by using the maxima of the slow gamma, the medium gamma, SG_{dom} events or the maxima in MG/SG ratio (MG_{dom} events). The inset shows examples of detected maxima in the four series types. *$p < 0.05$ relative to chance. Data are represented as average ± SEM.

We first investigated whether the occurrence of SG_{dom} events (avg. inter-event time 9.3 s) and putative avoidances (avg. inter-event time 26.0 s; Fig. 2B) were substantially similar or different (compare upper and lower time series in Fig. 2A). SG_{dom} events were more frequent than putative avoidances (Kolmogorov-Smirnov test $D_{3433} = 0.522$, $p < 0.001$) indicating that not every SG_{dom} event is followed by avoidance behavior. This means that while SG dominance in the CA1 LFP was initially identified by focusing on peri-avoidance episodes defined by stillness changing to locomotion, a parsimonious account for SG dominance is it is more likely to indicate moments of active recollection than just preparation for initiating movement (see supplementary information Video S1).

We then assessed the spatial distribution of SG_{dom} events (Fig. 2C). Consistent with these being internal, cognitive events, the spatial distribution of the SG_{dom} events resembles the spatial distribution of where the mice visited (maximal dwell opposite the shock zone; Kuiper's two-sample test compared

to dwell p = 1) and accordingly, these places differed from the places where the mice express avoidance behavior by initiating movement away from the leading edge of the shock zone (Kuiper's two-sample test compared to dwell p = 0.01). These data are consistent with SG_{dom} being related to an internal cognitive variable like active recollection, where recollection might not only be of the locations of shock.

We next studied in what behavioral states SG_{dom} events occur (Fig. 2D). SG_{dom} events occur during both active movement and stillness. Overall, they were similarly frequent during stillness and running (Fig. 2D) but less frequent in transitory behaviors from stillness to running or vice versa ($F_{4,44}$ = 6.25, p = 0.04; post-hoc Dunnett's test: still = run = other > still→run = run→still).

To further evaluate the possibility that SG dominance is indicative of long-term memory recollection, we tested the ability of the SG_{dom} events to predict successful avoidances, reasoning that recollecting locations of shock should precede effective avoidance behavior. First, we examined the probability of observing an avoidance at times relative to SG_{dom} events and compared that distribution to the probability of observing an avoidance at times relative to random events. The distributions were different and there was an increased occurrence of avoidances ~2 seconds after SG_{dom} events (Fig. 2E; Kolmogorov-Smirnov test D_{2715} = 0.08, p = 10^{-8}). Second, we created four avoidance predictors that used either the maxima in SG rate, maxima in MG rate, maxima in SG/MG ratio (i.e. SG_{dom}) or maxima in the MG/SG ratio (i.e. MG_{dom}). Prior to detecting these peaks, the ratios (SG/MG and MG/SG) were log-transformed and all time series were z-score normalized and only maxima with z-score values > 0.5 S.D were selected to guarantee similar rates of detected peaks in all four time series. Avoidances were predicted in a 4-s long window following the maxima. Note that even though the MG/SG ratio is the inverse of the SG/MG ratio, the maxima (i.e. SG_{dom} and MG_{dom}) in both series occur at different times (Fig. 2F inset). The four maxima types differed in their ability to predict avoidance (Fig. 2F; $F_{3,43}$ = 10.5, p < 0.0001); only the SG_{dom} had predictive power better than chance (t_8 = 24.56; P = 10^{-9}). While SG dominance occurred regularly and everywhere and during active and passive behavioral states, it

nonetheless predicts successful place avoidance, consistent with SG_{dom} signaling recollection of long-term memories.

Abnormal recollection in Fmr1-KO mice predicts excessive slow gamma dominance

We investigated the hypothesis that SG_{dom} events indicate long-term memory recollection by taking advantage of prior work with Fmr1-knockout (KO) mice [33]. These mice express a null form of the Fmr1 gene to model the genetic defect in FXS, a syndromic form of autism and the most common inherited form of intellectual disability [34]. Place avoidance learning and 24-h retention of long-term memory for the initial shock zone location appears normal in Fmr1-KO mice [33]. However, Fmr1-KO mice express cognitive inflexibility when they must avoid the formerly preferred place because the shock is relocated 180° on a conflict test (Fig. 3A). Whereas wild-type mice quickly adapt to the new location of shock on the conflict session, Fmr1-KO mice are impaired, possibly because they persist in recalling the former shock location that is now incorrect (Fig. 3B; Genotype: $F_{1,44} = 6.96$, $p = 0.01$; Session: $F_{1,44} = 77.32$, $p < 0.0001$; Time: $F_{1,44} = 48.62$, $p < 0.0001$; Genotype x Session x Time: $F_{1,44} = 11.16$, $p = 0.002$; Post-hoc tests confirm that WT and Fmr1-KO only differ in the second half of the conflict session).

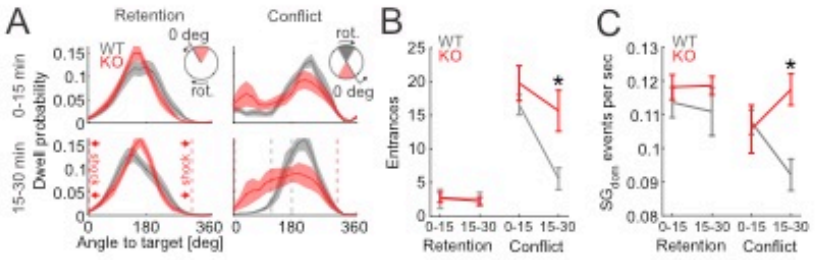

Figure 3. Cognitive inflexibility and associated increases in SG/MG maxima in Fmr1 KO mice A) Dwell distribution during first half (0-15 min; top) and second half (15-30 min; bottom) of retention (left) and conflict (right) sessions for wild-type and Fmr1-KO mice. Insets and dotted lines show locations of the active shock zone during each session (red) and location of the initial shock zone during conflict sessions

(gray). B) Behavioral performance during retention and conflict sessions for wild-type and Fmr1-KO mice. C) Rates of SG_{dom} events during retention and conflict sessions. *p < 0.05 between genotypes. Data are represented as average ± SEM.

We then examined if SG dominance distinguishes the wild-type and Fmr1-KO mice in the conflict session when the mutants express inflexibility relative to the wild-type mice. Whereas during the retention session and initial half of the conflict session the rate of SG_{dom} events was indistinguishable between the genotypes, the wild-type rate decreased in the second half of the conflict session while the Fmr1-KO rate appeared to increase, resulting in a significant Genotype x Time interaction ($F_{1,24}$ = 5.59, p = 0.027; Fig. 3C), and a marginal Genotype x Session x Time interaction ($F_{1,24}$ = 3.52, p = 0.07) because the genotypes only differed on the second half of the conflict session; no other effects were significant ($F_{1,24}$'s $\leq$ 1.71, p's > 0.2). These findings are consistent with the idea that SG dominance reflects recollection of long-term memories.

Slow gamma dominance predicts non-local place cell discharge during active place avoidance

Next, based on evidence that place cell discharge is more likely to represent non-local, distant places during recollection [35-37], we tested the hypothesis that SG dominance identifies recollection. The hypothesis predicts that during the place avoidance task, place cell discharge is non-local during SG dominance, assessed as increased error in the location estimate obtained from ensemble firing rates using a Bayesian decoder [38]. We examined CA1 place cell discharge from four wild-type and three Fmr1-KO mice after initial and conflict avoidance training. For these analyses, the SG_{dom} events were detected independently from all tetrodes on which place cells were identified. As predicted, during SG dominance, CA1 place cell discharge decodes to distant locations (Fig. 4). The example place cell ensemble recorded during active place avoidance (Fig. 4A) shows in Fig. 4B, that the error between the

observed and estimated locations is increased during the SG_{dom} events just prior to avoidance. We computed the average decoding error (z-score normalized difference between observed and decoded 1-D location) time-locked to the SG_{dom} events, during which we hypothesize recollection. For comparison, the decoding error was also computed time-locked to random moments as well as relative to FG_{dom} events (Fig. 4C). The Bayesian decoding error in both wild-type and Fmr1-KO mice was large around the time of SG_{dom} events, in contrast to the relatively small error associated with random times and with MG_{dom} events, during which the error was minimal (Fig. 4D). The decoding errors were greatest during SG_{dom} events ($F_{2,4215} = 7.87$, $p = 0.0004$; post-hoc Dunnett's test $SG_{dom} > MG_{dom} = RND$), and although this pattern appeared more extreme in Fmr1-KO mice at the time of the event, place representations in Fmr1-KO ensemble discharge did not differ from wild type (Genotype: $F_{1,4215} = 0.04$, $p = 0.9$; Genotype X Event Interaction: $F_{2,4215} = 0.33$, $p = 0.72$). This result could arise because the Bayesian posterior during SG_{dom} is less localized and thus more imprecise, or alternatively, during SG_{dom} the posterior could be just as compact as during non-SG_{dom} moments when place cell discharge decodes to current locations. The size of the posteriors were indistinguishable during SG_{dom}, MG_{dom}, and random moments when we decoded 2-D position ($F_{2,2127} = 0.74$, $p = 0.47$). In fact, the posteriors were most compact during SG_{dom} when we decoded the mouse's 1-D angle in the arena relative to the leading edge of the shock zone ($F_{2,2127} = 5.04$, $p = 0.006$; $SG_{dom} < MG_{dom} = RND$ according to post hoc Dunnett's tests), indicating the non-local representations of position during SG_{dom} were compact and precise, These findings confirm that place cell ensemble discharge selectively represents distant locations during SG dominance, consistent with recollection of locations remote from the mouse.

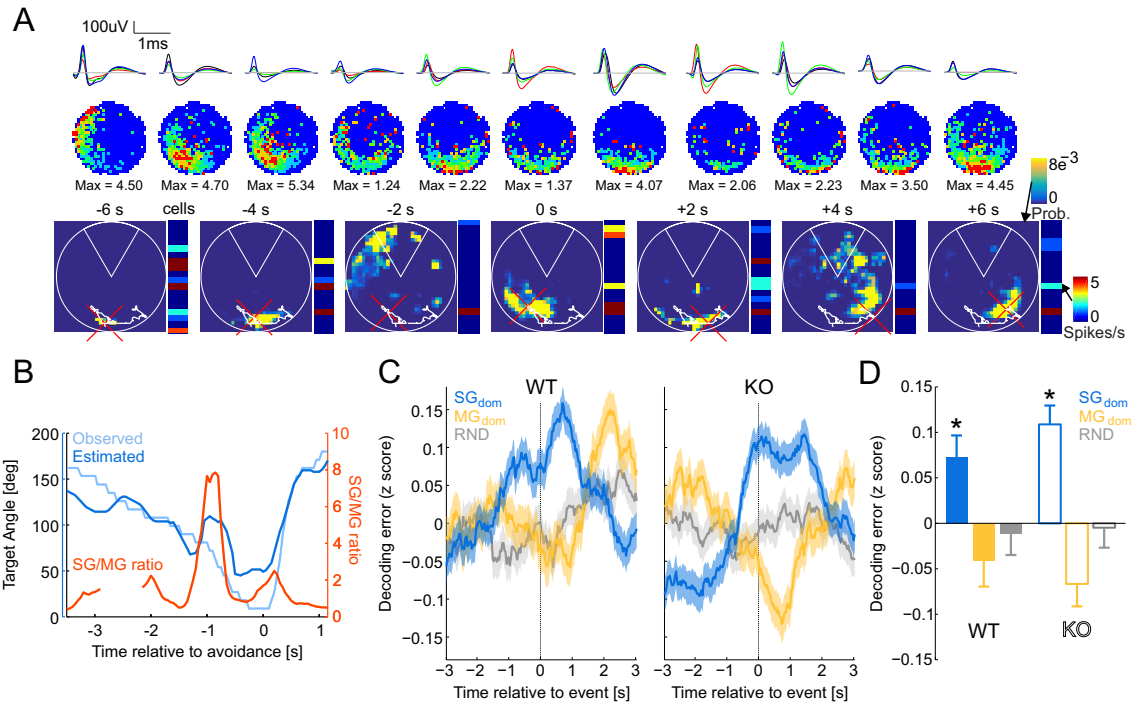

Figure 4. Error in Bayesian decoding of location increases during SG_{dom} events. A) Example firing rate maps (top) and 2-D decoded Bayesian posterior around avoidance onset. Ensemble activity vectors are shown to the right of each decoded Bayesian posterior. B) Time series of the angular position that was observed and decoded using a 1-D Bayesian estimator from ensemble discharge overlaid with the SG/MG ratio. Time T = 0 s marks avoidance onset. C) The average of wild-type (WT) and Fmr1 KO (KO) z-score normalized decoding error between observed and decoded locations from ensemble activity that is time-locked to SG_{dom} events, MG_{dom} events, and random times. Time T = 0 s corresponds to the time of the events. D) Summary of decoding error at the moments of SG_{dom} events, MG_{dom} events and random times (RND) for WT and KO mice. *p < 0.05 relative to random. Data are represented as average ± SEM.

Because of the role of sharp-wave ripple (SWR) events in replay of non-local place cell sequences [39], including during fear memory expression [40], we investigated this non-local decoding during isolated SG events (events detected in the 30-50 Hz band without concurrent MG or SWR events) and MG events (events detected in the 70-90 Hz band without concurrent SG or SWR events; see

supplementary material Fig. S4). This excluded the approximately 10% of SG and MG events that were concurrent with SWR events in both wild-type and Fmr1-KO mice (Fig. S4A). Both wild-type and Fmr1-KO place cell representations appeared more non-local during SG events compared to MG events, indicating that that events during sharp wave ripples cannot account for the observations (supplementary material Fig. S4C, D; Genotype: $F_{1,83264} = 0.03$, $p = 0.9$; Oscillation: $F_{1,83264} = 34.66$, $p < 0.0001$; Genotype x Oscillation Interaction: $F_{1,83264} = 2.02$, $p = 0.2$). These statistical tests included the ensemble firing rate as a covariate because of the significant relationships between decoding error and pyramidal cell firing rates (WT: $r^2 = 14\%$, $p < 0.0001$; Fmr1-KO: $r^2 = 8\%$, $p < 0.0001$), whereas speed explained substantially less of the variance (WT: $r^2 = 0.01\%$, $p < 0.0001$; Fmr1-KO: $r^2 = 0.4\%$, $p < 0.0001$). These findings with isolated slow gamma events, as well as those with slow gamma dominance, suggest that place memory recollection is predicted by slow gamma dominance, which also identifies when place cell ensembles will represent remote places, consistent with the hypothesis that slow gamma dominance in hippocampus CA1 identifies active recollection of long-term memory.

Place cell discharge during slow gamma dominance represents places that will be avoided

Finally, we analyzed the Bayesian posterior probability maps from the decoding to examine whether during avoidance sessions, place cell representations during SG dominance decode to the vicinity of the shock that the mouse will avoid, consistent with recollection of the places to avoid. Figure 5A shows four example Bayesian 2-D posterior probability maps computed at times before to times after individual avoidances. There are two examples from each genotype, one when the shock was in the initial location and the other after a conflict session with relocated shock. These examples illustrate that up until ~2 s before the avoidance, the peak values of the posterior probability correspond to the mouse's location. However, ~2 s before the avoidance of the initial shock location, in both genotypes, the posterior probability can peak at non-local positions that are in the vicinity of the shock zone or 180°

away, which is the safest and most frequented location on the arena during training to the initial shock location. The genotypes differ in the conflict session, remarkably. The wild-type example shows non-local decoding to the currently-correct, relocated shock location ~2 s before avoidance, whereas the Fmr1-KO example shows decoding to the currently-incorrect shock location that was formerly correct.

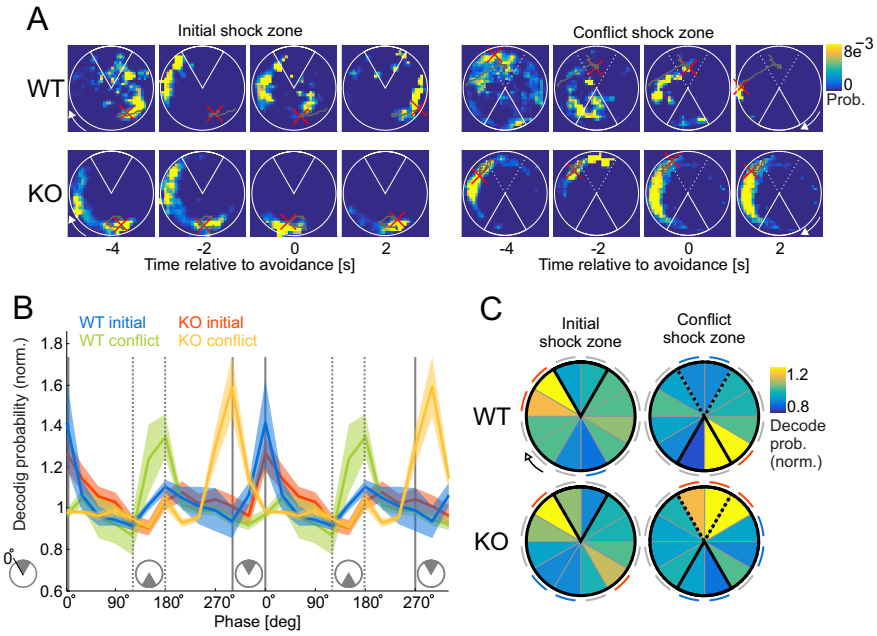

Figure 5. Place cell ensemble discharge during SG_{dom} events represent the vicinity of shock. A) Four examples of the time evolution of the Bayesian posterior probability from before to after avoiding the shock zone (white sector centered at 12 o'clock). The mouse's path during the episode is shown in gray with the current location indicated by a red cross. Top row corresponds to a wild-type mouse, bottom row to a Fmr1-KO mouse. The left examples illustrate training to the initial shock zone. The right examples are after the shock was relocated for conflict training. The initial shock zone location in conflict training shown as a dotted line. B) Average normalized posterior probability as a distance from the leading edge of the shock zone. The conflict session posterior probability distribution was rotated 180° to overlap with the initial shock zone session. Full gray lines mark the location of the initial shock zone, dotted lines mark location of the conflict shock zone. C) Summary of normalized posterior probability estimates obtained during SG_{dom} events for the initial (left) and conflict (right) shock zone sessions for

wild-type (top row) and Fmr1-KO (bottom row) mice. Notice maximal decoding probability at the leading edge of the shock zone in both WT and KO mice during the initial shock zone session, and during the conflict session, maximal decoding probability is at the leading edge of the relocated shock zone in WT mice but not in Fmr1-KO mice. During conflict, Fmr1-KO ensemble discharge decodes to the incorrect location of the initial shock zone. Red arcs located next to angular bins indicate significantly positive (>1) normalized probability ($p < 0.05$), blue arcs indicate significantly negative (<1) normalized probability ($p < 0.05$), gray arcs indicate n.s. relative to 1. Data are represented as averages ± SEM.

Similar patterns of representational flexibility in wild-type and inflexibility in Fmr1-KO are seen in the summary data, computed as the ratio of the posterior during SG_{dom} events normalized by the average posterior during MG_{dom} events, when decoding was local. During SG dominance, this posterior ratio peaks in the vicinity of the initial location of shock and this is observed for both wild-type and Fmr1-KO place cell representations (blue and red data in Fig. 5B, respectively). The posterior ratio peaks in the vicinity of the currently-correct location of shock in the post-conflict session, but only for wild-type place cell representations, demonstrating representational flexibility (green data in Fig. 5B). In the post-conflict session, the Fmr1-KO posterior ratio peaks adjacent to the currently-incorrect shock zone (yellow data in Fig. 5B). Statistical comparisons of the place cell posterior ratios confirm significant overrepresentation of the regions adjacent to the leading edge of the initial shock zone in the wild-type and Fmr1-KO mice. Overrepresentation is also observed at the relocated shock location in the conflict sessions, but only in wild-type place cell representations (Fig. 5C). Whereas, in Fmr1-KO place cell ensemble representations, the posterior ratios are overrepresented in the currently-incorrect shock location during the post-conflict sessions, as confirmed by the significant Genotype x Trial x Region interaction: $F_{11,36983} = 4.15$, $p < 0.0001$ (the main effects of Genotype and Trial were not significant but the effect of Region was significant $F_{11,36983} = 3.68$, $p < 0.0001$, the Genotype x Region interaction $F_{11,36983}$

= 2.59, p = 0.0027 and Trial x Region interactions were significant as well). These findings demonstrate that SG dominance corresponds to activation of non-local, memory-related place cell representations and demonstrate for the first time, representational inflexibility in Fmr1-KO mice concurrent with behavioral inflexibility (Fig. 3).

DISCUSSION

Summary – a neurophysiological hypotheses for recollection

To identify a neural signature of recollection, we selected an enriched sample of potential recollection events using behavioral criteria (Fig. 1) and investigated the rate of occurrence of gamma oscillations in the dorsal CA1 LFP. Individual slow and medium gamma events were not predictive, but SG dominance, i.e. maxima in the slow/medium ratio of event rates at *stratum pyramidale* predicted successful place avoidance (Fig. 2), suggesting SG dominance is a candidate neural signature of long-term memory recollection, at least for place memories. While wild-type mice attenuated SG dominance when it was necessary to suppress recollection of the initially learned locations of shock, SG dominance was not attenuated in Fmr1-KO mice when they demonstrate cognitive inflexibility (Fig. 3). SG dominance occurred approximately every 9 s in standard conditions of exploration as well as during place avoidance sessions, which is almost three times more frequent than active avoidance-like behaviors (Fig. 2). This indicates that if SG dominance corresponds to an internal variable like recollection, then it may not merely be the recollection of conditioning events such as locations of shock. Indeed, SG dominance coincides with non-local place cell representations during post-avoidance training sessions (Fig. 4). We note that although Fmr1-KO mice model the genetic defect in FXS and express a number of biochemical and synaptic abnormalities [41, 42] their place cells express normal place fields [43], which makes their cognitive flexibility deficits a challenge to explain. However, guided by the notion that SG dominance identifies long-term place memory recollection, we observed neural

representational inflexibility in Fmr1-KO mice, when they express behavioral inflexibility (Fig. 5). Together, these findings provide convergent evidence that SG dominance predicts recollection as well as abnormalities of recollection in Fmr1-KO mice. The findings are incompatible with the alternative possibility that SG dominance merely indicates a process that anticipates or prepares to initiate movement (Fig. 2). Although the SG_{dom} events were present during immobility they were not exclusive to immobility and they did not coincide with the recently described N-waves that are associated with local place representations during immobility [44]. Furthermore, after isolating slow-gamma oscillatory events from contamination by medium gamma events and sharp-wave ripples and correcting for firing rate bias of the decoding, slow gamma events still expressed non-local decoding (Supplementary material Fig. S4). Consequently, the SG_{dom} events may represent a complementary network state, in particular because unlike the N-waves, the discharge associated with SG_{dom} events is non-local (Fig. 4), consistent with the SG dominance signaling recollection of long-term memories of remote places and/or spatial events. By inspection, despite the non-local hippocampal representational discharge, SG dominance did not coincide with vicarious trial-and-error [45-47]. Place cell discharge is also non-local during sharp-wave associated ripple events during which sequences of place cell discharge from active behavior can be observed to replay [48-51]. This sharp-wave associated replay is thought to underlie memory consolidation and support memory and decision making during the initial stages of learning [44, 52, 53]. Because SG_{dom} events are distinct from this sharp-wave associated discharge, the SG_{dom} events represent different phenomena. Based on the present findings, we contend that SG dominance in the CA1 *stratum pyramidale* LFP is a neural signal that the hippocampus network is in the functional mode of recollecting long-term memories that are used to guide behavior, as in standard tests of long-term memory.

Implications for the routing by synchrony hypothesis

Identifying SG dominance as a neural signal of recollection was inspired by prior work that proposed slow gamma oscillations measured at *stratum pyramidale* correspond to recollection event-associated activity from the CA3 region into *stratum radiatum*, whereas the neocortical inputs to the *stratum lacunosum-moleculare* are associated with higher frequency gamma and carry information about what is currently being experienced for encoding [7, 12, 13]. This important idea offers a solution for how multiple types of place information might be routed to the hippocampus to be used judiciously [8, 36, 54], for example to solve place avoidance tasks on a rotating arena during which distinct representations of the same physical places are activated [55, 56]. However, careful analysis of the extracellular currents along the dendritic compartments of dorsal CA1 has not supported this basic proposition [57, 58]. CA1 gamma-organized spiking is not entrained to the gamma-organization of the inputs, and the discrete oscillatory events at the *stratum radiatum* and *stratum lacunosum-moleculare* compartments have frequency components that overlap in the slow and medium gamma frequency bands [Fig. S1; 14, 16, 33, 59]. Furthermore, these inputs are also relatively tonic, which has been both estimated [60] and observed during behavior [61, 62]. One factor that might add difficulty when interpreting differences in the literature is that most studies assume steady state cognitive conditions, which is not the case during either place avoidance or the foraging tasks that are often used, despite physical steady state conditions [55, 56, 63-65]. By selecting cognitively homogeneous samples, we find that recollection of hippocampus-dependent, actionable information is marked by the perisomatic region of CA1 being dominated by slow gamma over medium gamma oscillations, as if the two signals are in continuous competition (see Fig. S2). These SG dominance "recollection" events appear to require a relatively large decrease in medium gamma in coordination with a lesser or no decrease in slow gamma, possibly depending on task conditions (Fig. 1). Because medium gamma-associated entorhinal inputs facilitate CA1 spiking [14, 16], these observations point to a role for regulation of feed-forward inhibition in the competition between temporoammonic and Schaffer collateral inputs to CA1 [16, 27,

66-68]. The present observations suggest that recollection of long-term memory is a transient change in the balance of the two signals, that is rapidly followed by a reversal of the dominance of medium gamma by slow gamma. This result contrasts previous studies suggesting the appearance of one or the other type of gamma during processes of encoding and retrieval [7, 12, 13]. Contradictory observations that slow and medium gamma are commonly observed in the same theta cycle [Fig. S3; 14, 27] can be explained by the analyses that show the previously used thresholds of oscillation power selects for separate slow- and medium-preferring theta cycles (Fig. S3). While the present data do not support the details of the routing-by-synchrony hypothesis as first proposed [12, 13], the present findings support the gist, but without common feed-forward conceptions. Rather, this work has revealed dynamical operations within near continuous arrival of oscillation-associated inputs along the somato-dendritic compartments of CA1 [67]. This input engages excitation, inhibition, and disinhibition, and is integrated locally in dendrites, such that the discharge of CA1 principal cells occurs as if embedded within a local neural activity infrastructure from which their spiking can emerge when the local infrastructure permits, by its transient adjustments to create distinctive information processing modes, like encoding and recollection [59, 61, 69-73]. These transient adjustments appear to emerge through a complex interplay between local neural dynamics and afferent activity [54, 58, 67, 74], and while the rules of engagement for this competition remain unknown, they are neither merely, nor predominantly feed-forward [5, 69, 75, 76].

A neural signature of recollection

The recollection events we identified as perisomatic SG_{dom} events are brief, and they recur after several seconds, which may be a candidate mechanism for the seconds-long overdispersion dynamics in place representations that have been observed in single unit place cell ensemble studies during both place responding and foraging behaviors with no explicit cognitive demand [55, 56, 63, 64, 77]. Because

the time scales differ and the SG_{dom} events span several theta cycles, they are unlikely to be the same cognitive information processing mechanism that governs the sub-second dynamics of single place cell spiking that can be observed as rodents traverse a cell's place field and is interpreted as a form of encoding and recollection [7, 58, 78]. Rather the SG_{dom} events suggest that cognitive information processing is intimately tied to the coordinated regulation of inhibition at the perisomatic region, and perhaps elsewhere, under the control of the distinct, anatomically-segregated information-carrying afferents to CA1 [54, 59, 79], although the anatomical segregation of inputs may not be a requirement [67]. Resembling neural control of incompatible behaviors in leech [80], the present findings demonstrate in gamma a specific, dynamic coordination of excitation and inhibition that controls the cognitive information processing that permits effective spatial cognition, whereas its discoordination is associated with cognitive inflexibility [33, 54, 81]. Alterations in this coordination account for the cognitive effort of animal subjects both when they demonstrate adaptive cognitive information processing [14, 82] and when they exhibit inflexible cognition, as was observed in both the neural signals and the behavior of the wild-type and the Fmr1 KO mouse model of FXS and autism-related intellectual disability [33].

Experimental Procedures

All methods comply with the Public Health Service Policy on Humane Care and Use of Laboratory Animals and were approved by the New York University and State University of New York, Downstate Medical Center Institutional Animal Care and Use Committees. Because detailed methods have been described [31, 33], only brief descriptions are provided.

Subjects

A total of 21 wild-type mice with a mixed C57BL6/FVB background were used as well as 20

Fmr1-KO mice carrying the Fmr1^{tm1Cgr} allele on the same mixed C57BL6/FVB background. The mutant mice were obtained from Jackson Laboratories (Bar Harbor, ME) to establish local colonies. The mice were 3 - 6 months old. LFP recordings and behavior from 16 wild-type and 17 Fmr1-KO mice animals were studied in [33]. Of those mice, 9 wild-type mice were recorded during avoidance training with electrodes localized in *stratum pyramidale* and used for analyses in Figures 1 and 2. Seven wild-type mice and 9 Fmr1 KO mice were used for behavioral analyses of 24-h retention of place avoidance and conflict training (Fig. 3). Four wild-type mice and 6 Fmr1 KO mice with electrodes localized in *stratum pyramidale* were recorded during conflict training and used in electrophysiological analysis in Fig.3. Four wild-type mice and three Fmr1 KO mice were implanted with tetrodes and recorded after place avoidance training. These were used for the analyses in Figs. 4 and 5. One mouse was used for the CSD analysis in Fig. S2.

Surgery to implant electrodes

The LFP recordings from the 16 wild-type and 17 KO mice that were previously analyzed [33], were made from a bundle of six 75 µm Formvar-insulated NiCh wire electrodes (California Fine Wire, Grover Beach, CA), staggered by 170 µm, that were stereotaxically implanted under Nembutal anesthesia (60 mg/kg i.p.). The tip was aimed at -1.80 AP, $\pm$1.30 ML, -1.65 DV relative to bregma. The electrodes spanned the dorso-ventral axis of the dorsal hippocampus but the spacing was too great for current-source-density analyses. Reference electrodes were aimed at the cerebellar white matter. For single-unit recordings from 4 wild-type and 3 Fmr1 KO mice, an 8-tetrode, flexDrive (www.open-ephys.org) or a 4-tetrode custom drive was implanted under isoflurane anesthesia (2%, 1 L/min), with the electrodes aimed at the dorsal hippocampus [83], and bone screws, one of which served as a ground electrode. The electrode assemblies were anchored to the skull and bone screws with one of two dental

cements (Grip Cement, Dentsply, Milford DE and TEETs Denture Material, Co-oral-ite Dental MMG, Diamond Springs, CA). The mice were allowed at least 1 week to recover before experiments began.

Electrophysiological Recording

A custom unity-gain buffering preamplifier was connected to the electrode assembly and the electrophysiological signals were galvanically transmitted to the recording system by a light-weight counter-balanced cable. The differential signal from each electrode was low-pass filtered (600 Hz) and digitized at 2 kHz for LFPs and band-pass filtered (500 Hz – 6 kHz) and digitized at 48 kHz for action potentials using dacqUSB (Axona, St. Albans, U.K.). Two millisecond duration tetrode action potential waveforms were collected and stored for offline single unit isolation using custom software (Wclust; see supplementary information Fig. S4). Single unit isolation quality was quantified by computing $Isol_{BG}$ and $Isol_{NN}$ [84]. Single units (N = 455) were recorded and analyzed from 4 WT and 3 Fmr1 KO mice. Only 213 single units with both $Isol_{BG}$ and $Isol_{NN}$ greater than 4 bits were judged to be well-isolated and 124 of these were of sufficiently high quality place cells or non-spatial pyramidal cells for the present study, according to objective criteria (see supplementary information Fig. S5). LFPs were localized as previously described [33] or to CA1 *stratum pyramidale* because they showed LFP activity characteristic of *stratum pyramidale* and were recorded by the same electrode as place cells. The electrode locations were verified histologically at the end of recordings.

Active Place Avoidance

The active place avoidance task has been described in detail [85, 86] and the behavioral protocol was identical to [33]. Briefly, the mouse's position was tracked 30 times a second using an overhead camera and a PC-based video tracking system (Tracker, Bio-Signal Group, MA). All sessions lasted 30 minutes. Pretraining on the rotating (1 rpm) arena was followed 24-h afterwards by three training sessions during

which the mouse (n = 40) received a mild 0.2 mA, 60 Hz, 500 ms foot shock whenever it entered the shock zone. There was a 2-h rest in the home cage between training sessions. A subset of the mice received conflict training (n = 14) in which the conditions were identical to the training phase, except the shock zone was on the opposite side. The conflict task variant tests cognitive flexibility because the mice should suppress recollection of the initial memories of the location of shock so they can learn and use the new location of shock. Note that because the shock zone is unmarked, the physical conditions of all the sessions are identical except when the mouse is shocked, which is rare; for example, only for 10 s if a mouse receives 20 shocks during a 30-min session.

Data Analysis

Detection of behavioral events: During the first session of the initial training on the rotating arena, spatial behavior becomes stereotyped, with periods of stillness, when the mouse is passively carried towards the shock zone by the arena's rotation and periods of movement directed away from the shock zone. This is quantified when angular distance to the shock zone is plotted against time; it reveals a saw-tooth profile (Fig. 1B top). We selected two behavioral events based on the angular distance to the shock zone. The onset of avoidance (blue dots in Fig. 1B top) was defined as local minima in the target angle time series with preceding stillness without entering the shock zone. The second event was an escape (red dots in Fig. 1B top), defined as entrance to the shock zone with preceding stillness. To define stillness, speed was computed using 400 ms long sliding window. Stillness was identified as intervals with speed below 2cm/s. Brief crossings of the stillness threshold for less than 150 ms were not considered departures from stillness. Because some avoidances were preceded with the animal's initial acceleration towards the shock zone followed by a turn, local minima in the target angle time series occurred during speed above the stillness threshold, we included all avoidances with at least 1 s of stillness in a 3-s window prior to the detected avoidance onset.

Preprocessing for LFP recording quality: The LFP data were first processed by a custom artifact rejection algorithm, which marked continuous segments of artifact-free signals. Such segments that were 4 s or longer were used for further analysis. The majority of artifacts were related to the foot shock, specifically signal saturations and slowly changing DC signals as the recording system recovered from the shock artifact. Constant signals close to the maximal voltage of the analog-digital-convertor defined signal saturation. Periods of very low signal difference defined the slowly changing DC signal artifacts. Thresholds for an acceptable signal difference were selected by visual inspection, and used for analysis of the entire dataset. Each artifact segment was extended by 0.25 s on both sides and all artifact-free segments smaller than a 1-s minimum window were also discarded. Each channel in the dataset was processed independently and the algorithm performance was verified by visual inspection.

Detection of oscillatory events: A published algorithm was used to extract oscillatory events from the LFP independently for each recorded channel [31]. In the first step of the algorithm the LFP is transformed into a time-frequency power representation by convolving the LFP signal S with a group of complex Morlet wavelets resulting in complex band-specific representations $S_{f1}..S_{fN}$, where $f_1..f_N$ represent frequencies of interest (Fig. 1E). Instantaneous normalized power is then obtained by squaring the argument of the band-specific signal representation and dividing it by the square of the standard deviation of the band-specific signal such as $\frac{|X_{fi}|^2}{std(X_{fi})^2}$. In the next step, oscillatory events are detected as local peaks in the normalized 2-D time-frequency space (Supplementary information Fig. S2E). Band-specific oscillation rates are then computed as the number of detected events in a representative frequency bands (30-50 Hz for slow gamma, 70-90 Hz for medium gamma) with power exceeding a defined threshold (2.5 S.D. of the mean power) per unit of time (Refer to supplementary information Fig. S3 for the rationale for selecting power thresholds and representative frequency bands).

Calculation of instantaneous SG/MG ratio: First we extracted band-specific oscillatory rates in 1-s long windows advanced by 0.25 s. Next we smoothed the estimated rates of oscillatory events by 2.5-s long windows and took the ratio of SG (30-50 Hz) to MG (70-90 Hz) oscillatory rates. To obtain the maxima of the SG/MG ratio (SG_{dom} events), we searched for local maxima in the SG/MG series with peak prominence (amplitude difference between the maxima and preceding and following minima) of at least 1 and amplitude above 1 (corresponding to SG > MG). SG/MG minima (MG_{dom} events) were obtained in the same way by finding local maxima in the inverse MG/SG time series using the same prominence and amplitude setting (corresponding to SG < MG).

Bayesian analysis: To obtain estimates of the mouse's location based on single unit data, we used a published algorithm [38], where the probability of the current location is defined as $P(\boldsymbol{x}|\boldsymbol{n}) = C(\tau,\boldsymbol{n})P(\boldsymbol{x})\left(\prod_{i=1}^{N} f_i(\boldsymbol{x})^{n_i}\right)\exp\left(-\tau\sum_{i=1}^{N} f_i(\boldsymbol{x})\right)$, where $C(\tau,\boldsymbol{n})$ is a normalization factor so that $\sum_x P(\boldsymbol{x}|\boldsymbol{n}) = 1$, $f_i(\boldsymbol{x})$ are firing rate maps for cells *i..N* obtained either by binning the 2-D space into 32x32 bins or 1-D space (distance to shock zone) into 20 or 12 angular bins, $P(\boldsymbol{x})$ is the dwell distribution, τ is the length of the time window (500 or 200 ms), n_i is the number of spikes fired by the i-th cell in a given time window and $\boldsymbol{x}$ is the *(x,y)* position of the animal in the 2D analysis or the angular position in the 1D analysis. Only recordings with at least five high quality spatial or non-spatial pyramidal cells were analyzed. Time windows with no spikes were excluded from analysis. To obtain the error of the location estimate, we first computed the Euclidean distance between the observed location and every possible location represented by the location estimate $P(\boldsymbol{x}|\boldsymbol{n})$. We then multiplied $P(\boldsymbol{x}|\boldsymbol{n})$ by the Euclidean distances and took the average so location errors at highest probability will contribute proportionately more to the resulting error estimate. The resulting error estimate was z score normalized to account for absolute differences in the decoded error due to different numbers of place cells in a given recording.

AUTHOR CONTRIBUTIONS

D.D. analyzed the data, B.R. collected place avoidance and LFP data, F.T.S. and Z.N.T. collected single unit and associated place avoidance and LFP data, A.A.F. supervised research, and D.D. and A.A.F. designed the experiments and wrote the manuscript.

ACKNOWLEDGMENTS

This work was supported by a grant from the Simons Foundation (294388, A.A.F.), a grant from NIH (R01MH099128) and a CIHR Fellowship to F.T.S.

REFERENCES

1. O'Keefe J, Nadel L. The hippocampus as a cognitive map. Oxford: Clarendon Press; 1978. xiv, 570 p. p.
2. Mehta MR, Barnes CA, McNaughton BL. Experience-dependent, asymmetric expansion of hippocampal place fields. Proc Natl Acad Sci U S A. 1997;94(16):8918-21. Epub 1997/08/05. PubMed PMID: 9238078.
3. Lever C, Wills T, Cacucci F, Burgess N, O'Keefe J. Long-term plasticity in hippocampal place-cell representation of environmental geometry. Nature. 2002;416(6876):90-4. Epub 2002/03/08. doi: 10.1038/416090a
416090a [pii]. PubMed PMID: 11882899.
4. Ji D, Wilson MA. Firing rate dynamics in the hippocampus induced by trajectory learning. J Neurosci. 2008;28(18):4679-89. Epub 2008/05/02. doi: 28/18/4679 [pii]
10.1523/JNEUROSCI.4597-07.2008. PubMed PMID: 18448645.
5. Dragoi G, Tonegawa S. Distinct preplay of multiple novel spatial experiences in the rat. Proc Natl Acad Sci U S A. 2013;110(22):9100-5. Epub 2013/05/15. doi: 1306031110 [pii]
10.1073/pnas.1306031110. PubMed PMID: 23671088; PubMed Central PMCID: PMC3670374.
6. Ramirez S, Liu X, Lin PA, Suh J, Pignatelli M, Redondo RL, et al. Creating a false memory in the hippocampus. Science. 2013;341(6144):387-91. Epub 2013/07/28. doi: 341/6144/387 [pii]
10.1126/science.1239073. PubMed PMID: 23888038.
7. Bieri KW, Bobbitt KN, Colgin LL. Slow and fast gamma rhythms coordinate different spatial coding modes in hippocampal place cells. Neuron. 2014;82(3):670-81. Epub 2014/04/22. doi: S0896-6273(14)00241-4 [pii]

10.1016/j.neuron.2014.03.013. PubMed PMID: 24746420.
8. Carr MF, Frank LM. A single microcircuit with multiple functions: state dependent information processing in the hippocampus. Curr Opin Neurobiol. 2012;22(4):704-8. doi: 10.1016/j.conb.2012.03.007. PubMed PMID: 22480878; PubMed Central PMCID: PMCPMC3438355.
9. Fries P. Neuronal gamma-band synchronization as a fundamental process in cortical computation. Annu Rev Neurosci. 2009;32:209-24. Epub 2009/04/30. doi: 10.1146/annurev.neuro.051508.135603. PubMed PMID: 19400723.
10. Akam TE, Kullmann DM. Efficient "communication through coherence" requires oscillations structured to minimize interference between signals. PLoS Comput Biol. 2012;8(11):e1002760. doi: 10.1371/journal.pcbi.1002760. PubMed PMID: 23144603; PubMed Central PMCID: PMCPMC3493486.
11. Akam T, Kullmann DM. Oscillatory multiplexing of population codes for selective communication in the mammalian brain. Nat Rev Neurosci. 2014;15(2):111-22. doi: 10.1038/nrn3668. PubMed PMID: 24434912; PubMed Central PMCID: PMCPMC4724886.
12. Colgin LL, Denninger T, Fyhn M, Hafting T, Bonnevie T, Jensen O, et al. Frequency of gamma oscillations routes flow of information in the hippocampus. Nature. 2009;462(7271):353-7. Epub 2009/11/20. doi: nature08573 [pii]
10.1038/nature08573. PubMed PMID: 19924214.
13. Fries P. The model- and the data-gamma. Neuron. 2009;64(5):601-2. Epub 2009/12/17. doi: S0896-6273(09)00940-4 [pii]
10.1016/j.neuron.2009.11.024. PubMed PMID: 20005817.
14. Schomburg EW, Fernandez-Ruiz A, Mizuseki K, Berenyi A, Anastassiou CA, Koch C, et al. Theta phase segregation of input-specific gamma patterns in entorhinal-hippocampal networks. Neuron. 2014;84(2):470-85. Epub 2014/09/30. doi: S0896-6273(14)00781-8 [pii]
10.1016/j.neuron.2014.08.051. PubMed PMID: 25263753.
15. Whittington MA, Traub RD, Jefferys JG. Synchronized oscillations in interneuron networks driven by metabotropic glutamate receptor activation. Nature. 1995;373(6515):612-5. Epub 1995/02/16. doi: 10.1038/373612a0. PubMed PMID: 7854418.
16. Lasztoczi B, Klausberger T. Layer-Specific GABAergic Control of Distinct Gamma Oscillations in the CA1 Hippocampus. Neuron. 2014;81(5):1126-39. Epub 2014/03/13. doi: S0896-6273(14)00052-X [pii]
10.1016/j.neuron.2014.01.021. PubMed PMID: 24607232.
17. Csicsvari J, Jamieson B, Wise KD, Buzsaki G. Mechanisms of gamma oscillations in the hippocampus of the behaving rat. Neuron. 2003;37(2):311-22. Epub 2003/01/28. doi: S0896627302011698 [pii]. PubMed PMID: 12546825.
18. Whittington MA, Traub RD, Kopell N, Ermentrout B, Buhl EH. Inhibition-based rhythms: experimental and mathematical observations on network dynamics. Int J Psychophysiol. 2000;38(3):315-36. Epub 2000/12/05. doi: S0167876000001732 [pii]. PubMed PMID: 11102670.
19. Buzsaki G, Wang XJ. Mechanisms of gamma oscillations. Annu Rev Neurosci. 2012;35:203-25. doi: 10.1146/annurev-neuro-062111-150444. PubMed PMID: 22443509; PubMed Central PMCID: PMCPMC4049541.
20. Zemankovics R, Veres JM, Oren I, Hajos N. Feedforward inhibition underlies the propagation of cholinergically induced gamma oscillations from hippocampal CA3 to CA1. J Neurosci. 2013;33(30):12337-51. doi: 10.1523/JNEUROSCI.3680-12.2013. PubMed PMID: 23884940; PubMed Central PMCID: PMCPMC3721843.
21. Keeley S, Fenton AA, Rinzel J. Modeling Fast and Slow Gamma Oscillations with Interneurons of Different Subtype. J Neurophysiol. 2016:jn 00490 2016. doi: 10.1152/jn.00490.2016. PubMed PMID: 27927782.

22. Amaral DG, Witter MP. The three-dimensional organization of the hippocampal formation: a review of anatomical data. Neuroscience. 1989;31(3):571-91. Epub 1989/01/01. doi: 0306-4522(89)90424-7 [pii]. PubMed PMID: 2687721.
23. Witter MP, Groenewegen HJ, Lopes da Silva FH, Lohman AH. Functional organization of the extrinsic and intrinsic circuitry of the parahippocampal region. Prog Neurobiol. 1989;33(3):161-253. Epub 1989/01/01. doi: 0301-0082(89)90009-9 [pii]. PubMed PMID: 2682783.
24. Buzsaki G. Feed-forward inhibition in the hippocampal formation. Prog Neurobiol. 1984;22(2):131-53. Epub 1984/01/01. doi: 0301-0082(84)90023-6 [pii]. PubMed PMID: 6433403.
25. Cimadevilla JM, Wesierska M, Fenton AA, Bures J. Inactivating one hippocampus impairs avoidance of a stable room-defined place during dissociation of arena cues from room cues by rotation of the arena. Proc Natl Acad Sci U S A. 2001;98(6):3531-6. Epub 2001/03/15. doi: 10.1073/pnas.051628398
98/6/3531 [pii]. PubMed PMID: 11248112.
26. Kelemen E, Moron I, Fenton AA. Is the hippocampal theta rhythm related to cognition in a non-locomotor place recognition task? Hippocampus. 2005;15(4):472-9. Epub 2005/03/04. doi: 10.1002/hipo.20071. PubMed PMID: 15744737.
27. Lasztoczi B, Klausberger T. Hippocampal Place Cells Couple to Three Different Gamma Oscillations during Place Field Traversal. Neuron. 2016;91(1):34-40. doi: 10.1016/j.neuron.2016.05.036. PubMed PMID: 27387648.
28. Fernandez-Ruiz A, Herreras O. Identifying the synaptic origin of ongoing neuronal oscillations through spatial discrimination of electric fields. Front Comput Neurosci. 2013;7:5. doi: 10.3389/fncom.2013.00005. PubMed PMID: 23408586; PubMed Central PMCID: PMCPMC3569616.
29. Chen Z, Resnik E, McFarland JM, Sakmann B, Mehta MR. Speed controls the amplitude and timing of the hippocampal gamma rhythm. PLoS One. 2011;6(6):e21408. Epub 2011/07/07. doi: 10.1371/journal.pone.0021408
PONE-D-11-05752 [pii]. PubMed PMID: 21731735; PubMed Central PMCID: PMC3123337.
30. Buzsaki G, Mizuseki K. The log-dynamic brain: how skewed distributions affect network operations. Nat Rev Neurosci. 2014;15(4):264-78. Epub 2014/02/27. doi: nrn3687 [pii] 10.1038/nrn3687. PubMed PMID: 24569488; PubMed Central PMCID: PMC4051294.
31. Dvorak D, Fenton AA. Toward a proper estimation of phase-amplitude coupling in neural oscillations. J Neurosci Methods. 2014;225C:42-56. Epub 2014/01/23. doi: S0165-0270(14)00013-2 [pii] 10.1016/j.jneumeth.2014.01.002. PubMed PMID: 24447842.
32. Zheng C, Bieri KW, Hwaun E, Colgin LL. Fast Gamma Rhythms in the Hippocampus Promote Encoding of Novel Object-Place Pairings. eNeuro. 2016;3(2). doi: 10.1523/ENEURO.0001-16.2016. PubMed PMID: 27257621; PubMed Central PMCID: PMCPMC4874540.
33. Radwan B, Dvorak D, Fenton A. Impaired cognitive discrimination and discoordination of coupled theta-gamma oscillations in Fmr1 knockout mice. Neurobiol Dis. 2016. doi: 10.1016/j.nbd.2016.01.003. PubMed PMID: 26792400.
34. Pieretti M, Zhang FP, Fu YH, Warren ST, Oostra BA, Caskey CT, et al. Absence of expression of the FMR-1 gene in fragile X syndrome. Cell. 1991;66(4):817-22. Epub 1991/08/23. doi: 0092-8674(91)90125-I [pii]. PubMed PMID: 1878973.
35. Gupta AS, van der Meer MA, Touretzky DS, Redish AD. Hippocampal replay is not a simple function of experience. Neuron. 2010;65(5):695-705. Epub 2010/03/13. doi: S0896-6273(10)00060-7 [pii]
10.1016/j.neuron.2010.01.034. PubMed PMID: 20223204.
36. Carr MF, Karlsson MP, Frank LM. Transient slow gamma synchrony underlies hippocampal memory replay. Neuron. 2012;75(4):700-13. Epub 2012/08/28. doi: S0896-6273(12)00576-4 [pii] 10.1016/j.neuron.2012.06.014. PubMed PMID: 22920260; PubMed Central PMCID: PMC3428599.

37. Karlsson MP, Frank LM. Awake replay of remote experiences in the hippocampus. Nat Neurosci. 2009;12(7):913-8. Epub 2009/06/16. doi: nn.2344 [pii]
10.1038/nn.2344. PubMed PMID: 19525943; PubMed Central PMCID: PMC2750914.
38. Zhang K, Ginzburg I, McNaughton BL, Sejnowski TJ. Interpreting neuronal population activity by reconstruction: unified framework with application to hippocampal place cells. J Neurophysiol. 1998;79(2):1017-44. Epub 1998/04/18. PubMed PMID: 9463459.
39. Carr MF, Jadhav SP, Frank LM. Hippocampal replay in the awake state: a potential substrate for memory consolidation and retrieval. Nat Neurosci. 2011;14(2):147-53. Epub 2011/01/29. doi: nn.2732 [pii]
10.1038/nn.2732. PubMed PMID: 21270783; PubMed Central PMCID: PMC3215304.
40. Wu CT, Haggerty D, Kemere C, Ji D. Hippocampal awake replay in fear memory retrieval. Nat Neurosci. 2017;20(4):571-80. doi: 10.1038/nn.4507. PubMed PMID: 28218916; PubMed Central PMCID: PMCPMC5373994.
41. Zhang J, Hou L, Klann E, Nelson DL. Altered hippocampal synaptic plasticity in the FMR1 gene family knockout mouse models. J Neurophysiol. 2009;101(5):2572-80. Epub 2009/02/27. doi: 90558.2008 [pii]
10.1152/jn.90558.2008. PubMed PMID: 19244359; PubMed Central PMCID: PMC2681424.
42. Bhakar AL, Dolen G, Bear MF. The pathophysiology of fragile X (and what it teaches us about synapses). Annu Rev Neurosci. 2012;35:417-43. Epub 2012/04/10. doi: 10.1146/annurev-neuro-060909-153138. PubMed PMID: 22483044.
43. Sparks FT, Talbot ZN, Dvorak D, Fenton AA. Normal place fields but hyper stable temporal coordination within the CA1 network of a mouse model of Fragile X Syndrome. in review.
44. Kay K, Sosa M, Chung JE, Karlsson MP, Larkin MC, Frank LM. A hippocampal network for spatial coding during immobility and sleep. Nature. 2016;531:185-90. doi: 10.1038/nature17144.
45. Redish AD. Vicarious trial and error. Nat Rev Neurosci. 2016;17(3):147-59. Epub 2016/02/20. doi: nrn.2015.30 [pii]
10.1038/nrn.2015.30. PubMed PMID: 26891625.
46. Tolman EC. Prediction of vicarious trial and error by means of the schematic sowbug. Psychological ReviewPsychological Review. 1939;46:318–36.
47. Papale AE, Zielinski MC, Frank LM, Jadhav SP, Redish AD. Interplay between Hippocampal Sharp-Wave-Ripple Events and Vicarious Trial and Error Behaviors in Decision Making. Neuron. 2016;92(5):975-82. doi: 10.1016/j.neuron.2016.10.028. PubMed PMID: 27866796; PubMed Central PMCID: PMCPMC5145752.
48. O'Neill J, Senior T, Csicsvari J. Place-selective firing of CA1 pyramidal cells during sharp wave/ripple network patterns in exploratory behavior. Neuron. 2006;49(1):143-55. Epub 2006/01/03. doi: S0896-6273(05)00961-X [pii]
10.1016/j.neuron.2005.10.037. PubMed PMID: 16387646.
49. Jackson JC, Johnson A, Redish AD. Hippocampal sharp waves and reactivation during awake states depend on repeated sequential experience. J Neurosci. 2006;26(48):12415-26. Epub 2006/12/01. doi: 26/48/12415 [pii]
10.1523/JNEUROSCI.4118-06.2006. PubMed PMID: 17135403.
50. Csicsvari J, Hirase H, Mamiya A, Buzsaki G. Ensemble patterns of hippocampal CA3-CA1 neurons during sharp wave-associated population events. Neuron. 2000;28(2):585-94. Epub 2001/01/06. doi: S0896-6273(00)00135-5 [pii]. PubMed PMID: 11144366.
51. Buzsaki G. Hippocampal sharp waves: their origin and significance. Brain Res. 1986;398(2):242-52. Epub 1986/11/29. doi: 0006-8993(86)91483-6 [pii]. PubMed PMID: 3026567.

52. Singer AC, Carr MF, Karlsson MP, Frank LM. Hippocampal SWR activity predicts correct decisions during the initial learning of an alternation task. Neuron. 2013;77(6):1163-73. Epub 2013/03/26. doi: S0896-6273(13)00093-7 [pii]
10.1016/j.neuron.2013.01.027. PubMed PMID: 23522050; PubMed Central PMCID: PMC3751175.
53. Buzsaki G. Hippocampal sharp wave-ripple: A cognitive biomarker for episodic memory and planning. Hippocampus. 2015;25(10):1073-188. doi: 10.1002/hipo.22488. PubMed PMID: 26135716; PubMed Central PMCID: PMCPMC4648295.
54. Cabral HO, Vinck M, Fouquet C, Pennartz CM, Rondi-Reig L, Battaglia FP. Oscillatory dynamics and place field maps reflect hippocampal ensemble processing of sequence and place memory under NMDA receptor control. Neuron. 2014;81(2):402-15. Epub 2014/01/28. doi: S0896-6273(13)01044-1 [pii]
10.1016/j.neuron.2013.11.010. PubMed PMID: 24462101.
55. Kelemen E, Fenton AA. Key features of human episodic recollection in the cross-episode retrieval of rat hippocampus representations of space. PLoS Biol. 2013;11(7):e1001607.
56. Kelemen E, Fenton AA. Dynamic grouping of hippocampal neural activity during cognitive control of two spatial frames. PLoS Biol. 2010;8(6):e1000403. Epub 2010/06/30. doi: 10.1371/journal.pbio.1000403. PubMed PMID: 20585373; PubMed Central PMCID: PMC2889929.
57. Buzsaki G, Schomburg EW. What does gamma coherence tell us about inter-regional neural communication? Nat Neurosci. 2015;18(4):484-9. doi: 10.1038/nn.3952. PubMed PMID: 25706474.
58. Fernandez-Ruiz A, Oliva A, Nagy GA, Maurer AP, Berenyi A, Buzsaki G. Entorhinal-CA3 Dual-Input Control of Spike Timing in the Hippocampus by Theta-Gamma Coupling. Neuron. 2017;93(5):1213-26 e5. doi: 10.1016/j.neuron.2017.02.017. PubMed PMID: 28279355.
59. Basu J, Zaremba JD, Cheung SK, Hitti FL, Zemelman BV, Losonczy A, et al. Gating of hippocampal activity, plasticity, and memory by entorhinal cortex long-range inhibition. Science. 2016;351(6269):aaa5694. doi: 10.1126/science.aaa5694. PubMed PMID: 26744409.
60. Olypher AV, Lansky P, Fenton AA. Properties of the extra-positional signal in hippocampal place cell discharge derived from the overdispersion in location-specific firing. Neuroscience. 2002;111(3):553-66. Epub 2002/05/29. doi: S0306452201005863 [pii]. PubMed PMID: 12031343.
61. Bittner KC, Grienberger C, Vaidya SP, Milstein AD, Macklin JJ, Suh J, et al. Conjunctive input processing drives feature selectivity in hippocampal CA1 neurons. Nat Neurosci. 2015;18(8):1133-42. doi: 10.1038/nn.4062. PubMed PMID: 26167906.
62. Grienberger C, Milstein AD, Bittner KC, Romani S, Magee JC. Inhibitory suppression of heterogeneously tuned excitation enhances spatial coding in CA1 place cells. Nat Neurosci. 2017;20(3):417-26. doi: 10.1038/nn.4486. PubMed PMID: 28114296.
63. Fenton AA, Lytton WW, Barry JM, Lenck-Santini PP, Zinyuk LE, Kubik S, et al. Attention-like modulation of hippocampus place cell discharge. J Neurosci. 2010;30(13):4613-25. Epub 2010/04/02. doi: 30/13/4613 [pii]
10.1523/JNEUROSCI.5576-09.2010. PubMed PMID: 20357112.
64. Jackson J, Redish AD. Network dynamics of hippocampal cell-assemblies resemble multiple spatial maps within single tasks. Hippocampus. 2007;17(12):1209-29. Epub 2007/09/04. doi: 10.1002/hipo.20359. PubMed PMID: 17764083.
65. Kelemen E, Fenton AA. Coordinating different representations in the hippocampus. Neurobiol Learn Mem. 2016;129:50-9. doi: 10.1016/j.nlm.2015.12.011. PubMed PMID: 26748023.
66. Somogyi P, Katona L, Klausberger T, Lasztoczi B, Viney TJ. Temporal redistribution of inhibition over neuronal subcellular domains underlies state-dependent rhythmic change of excitability in the hippocampus. Philos Trans R Soc Lond B Biol Sci. 2014;369(1635):20120518. doi: 10.1098/rstb.2012.0518. PubMed PMID: 24366131; PubMed Central PMCID: PMCPMC3866441.

67. Rajan K, Harvey CD, Tank DW. Recurrent Network Models of Sequence Generation and Memory. Neuron. 2016;90(1):128-42. doi: 10.1016/j.neuron.2016.02.009. PubMed PMID: 26971945; PubMed Central PMCID: PMCPMC4824643.
68. Leao RN, Mikulovic S, Leao KE, Munguba H, Gezelius H, Enjin A, et al. OLM interneurons differentially modulate CA3 and entorhinal inputs to hippocampal CA1 neurons. Nat Neurosci. 2012;15(11):1524-30. doi: 10.1038/nn.3235. PubMed PMID: 23042082; PubMed Central PMCID: PMC3483451.
69. Stark E, Roux L, Eichler R, Buzsaki G. Local generation of multineuronal spike sequences in the hippocampal CA1 region. Proc Natl Acad Sci U S A. 2015;112(33):10521-6. doi: 10.1073/pnas.1508785112. PubMed PMID: 26240336; PubMed Central PMCID: PMCPMC4547251.
70. Buzsaki G. Neural syntax: cell assemblies, synapsembles, and readers. Neuron. 2010;68(3):362-85. Epub 2010/11/03. doi: S0896-6273(10)00765-8 [pii] 10.1016/j.neuron.2010.09.023. PubMed PMID: 21040841; PubMed Central PMCID: PMC3005627.
71. Rickgauer JP, Deisseroth K, Tank DW. Simultaneous cellular-resolution optical perturbation and imaging of place cell firing fields. Nat Neurosci. 2014;17(12):1816-24. doi: 10.1038/nn.3866. PubMed PMID: 25402854; PubMed Central PMCID: PMCPMC4459599.
72. Traub RD, Spruston N, Soltesz I, Konnerth A, Whittington MA, Jefferys GR. Gamma-frequency oscillations: a neuronal population phenomenon, regulated by synaptic and intrinsic cellular processes, and inducing synaptic plasticity. Prog Neurobiol. 1998;55(6):563-75. Epub 1998/07/22. doi: S0301008298000203 [pii]. PubMed PMID: 9670218.
73. Stuart GJ, Spruston N. Dendritic integration: 60 years of progress. Nat Neurosci. 2015;18(12):1713-21. doi: 10.1038/nn.4157. PubMed PMID: 26605882.
74. Lundqvist M, Rose J, Herman P, Brincat SL, Buschman TJ, Miller EK. Gamma and Beta Bursts Underlie Working Memory. Neuron. 2016;90(1):152-64. doi: 10.1016/j.neuron.2016.02.028. PubMed PMID: 26996084.
75. Pastalkova E, Itskov V, Amarasingham A, Buzsaki G. Internally generated cell assembly sequences in the rat hippocampus. Science. 2008;321(5894):1322-7. Epub 2008/09/06. doi: 321/5894/1322 [pii] 10.1126/science.1159775. PubMed PMID: 18772431.
76. MacDonald CJ, Lepage KQ, Eden UT, Eichenbaum H. Hippocampal "time cells" bridge the gap in memory for discontiguous events. Neuron. 2011;71(4):737-49. Epub 2011/08/27. doi: S0896-6273(11)00609-X [pii] 10.1016/j.neuron.2011.07.012. PubMed PMID: 21867888; PubMed Central PMCID: PMC3163062.
77. Kelemen E, Fenton AA. Coordinating different representations in the hippocampus. Neurobiol Learn Mem. 2015. doi: 10.1016/j.nlm.2015.12.011. PubMed PMID: 26748023.
78. Zheng C, Bieri KW, Hsiao YT, Colgin LL. Spatial Sequence Coding Differs during Slow and Fast Gamma Rhythms in the Hippocampus. Neuron. 2016;89(2):398-408. doi: 10.1016/j.neuron.2015.12.005. PubMed PMID: 26774162; PubMed Central PMCID: PMCPMC4731025.
79. Royer S, Zemelman BV, Losonczy A, Kim J, Chance F, Magee JC, et al. Control of timing, rate and bursts of hippocampal place cells by dendritic and somatic inhibition. Nat Neurosci. 2012;15(5):769-75. Epub 2012/03/27. doi: nn.3077 [pii] 10.1038/nn.3077. PubMed PMID: 22446878.
80. Briggman KL, Abarbanel HD, Kristan WB, Jr. Optical imaging of neuronal populations during decision-making. Science. 2005;307(5711):896-901. Epub 2005/02/12. doi: 307/5711/896 [pii] 10.1126/science.1103736. PubMed PMID: 15705844.
81. Fenton AA. Excitation-inhibition discoordination in rodent models of mental disorders. Biol Psychiatry. 2015;77(12):1079-88. doi: 10.1016/j.biopsych.2015.03.013. PubMed PMID: 25895430; PubMed Central PMCID: PMCPMC4444398.

82. Montgomery SM, Buzsaki G. Gamma oscillations dynamically couple hippocampal CA3 and CA1 regions during memory task performance. Proc Natl Acad Sci U S A. 2007;104(36):14495-500. Epub 2007/08/30. doi: 0701826104 [pii]
10.1073/pnas.0701826104. PubMed PMID: 17726109.
83. Voigts J, Siegle JH, Pritchett DL, Moore CI. The flexDrive: an ultra-light implant for optical control and highly parallel chronic recording of neuronal ensembles in freely moving mice. Front Syst Neurosci. 2013;7:8. doi: 10.3389/fnsys.2013.00008. PubMed PMID: 23717267; PubMed Central PMCID: PMCPMC3652307.
84. Neymotin SA, Lytton WW, Olypher AV, Fenton AA. Measuring the Quality of Neuronal Identification in Ensemble Recordings. J Neurosci. 2011;31(45):16398-409. Epub 2011/11/11. doi: 31/45/16398 [pii]
10.1523/JNEUROSCI.4053-11.2011. PubMed PMID: 22072690.
85. Kheirbek MA, Drew LJ, Burghardt NS, Costantini DO, Tannenholz L, Ahmari SE, et al. Differential Control of Learning and Anxiety along the Dorsoventral Axis of the Dentate Gyrus. Neuron. 2013;77(5):955-68. Epub 2013/03/12. doi: S0896-6273(13)00046-9 [pii]
10.1016/j.neuron.2012.12.038. PubMed PMID: 23473324; PubMed Central PMCID: PMC3595120.
86. Burghardt NS, Park EH, Hen R, Fenton AA. Adult-born hippocampal neurons promote cognitive flexibility in mice. Hippocampus. 2012;22(9):1795-808. Epub 2012/03/21. doi: 10.1002/hipo.22013. PubMed PMID: 22431384.